THREE-DIMENSIONAL PARTICLE IMAGE VELOCIMETRY IN A GENERIC CAN-TYPE GAS TURBINE COMBUSTOR

BC Meyers*, GC Snedden**, JP Meyer*, TH Roos**, GI Mahmood*
*University of Pretoria, Department of Mechanical and Aeronautical Engineering,
Pretoria, South Africa
**CSIR, DPSS, PO Box 395, Pretoria, 0001, South Africa
bmeyers@csir.co.za (BC Meyers)

Abstract

The three-dimensional flow field inside a generic can-type, forward flow, experimental combustor was measured. A stereoscopic Particle Image Velocimetry (PIV) system was used to obtain the flow field of the combustor in the non-reacting condition. In order for these measurements to be taken, an optically accessible combustor was manufactured. Contour maps of the velocity magnitude is shown which indicates the jet penetration depths while the streamlines show the recirculation zones and flow paths taken by the bulk flow from all inlets to the exit plane. Velocity vectors show the swirling action and the three-dimensional nature of the flow inside a combustor. This data can be used effectively as a test case for Computational Fluid Dynamics (CFD) studies due to the presence of all the flow features of the combustor.

Nomenclature

Symbols

Δp	Pressure Difference
Φ	Diameter
T	Temperature
p	Static Pressure

Abbreviations

3D	Three-Dimensional
4M	4 Megapixel
CCD	Charged Couple Device
CFD	Computational Fluid Dynamics
ID	Inner Diameter
LDV	Laser Doppler Velocimetry
PIV	Particle Image Velocimetry
Vel	Velocity
Mag	Magnitude

Subscripts

1	Fan Outlet
3	Combustor Inlet
L	(Combustor) Liner
OP	Orifice Plate

Introduction

For gas turbine combustors, it is a general problem that there are many inconsistencies between experimental work and CFD solutions [1, 2]. Combustion CFD solutions often compare poorly with experimental values owing to inaccuracies in both flow modeling as well as combustion modeling.

The purpose of this study was to collect data that can be used to validate CFD results in order to ensure that CFD can be used as a reliable design tool for gas turbine combustors. The design of a combustor could entail simulations in order to prove or test a specific combustor setup or the optimisation of a preliminary design [2, 3, 4]. The data could also be used as a test case for new CFD models. A steady state experimental test case has been created for these purposes.

In most CFD cases a non-reacting run is done first in order to ensure the turbulence model is predicting the flow field and the position of the important flow phenomena correctly [1, 3]. This step is important because the combustion characteristics and the correctness of the reacting flow results are dependent on the flow characteristics [2, 5]. The flow field within an atmospheric pressure gas turbine combustor was measured using a stereoscopic PIV system in order to validate this step in the modelling process. Once the non-reacting flow has been modelled satisfactorily the reacting flow can then be modelled.

Similar to Carl *et al.* [6], this study attempts to ensure that as many of the factors that influence the combustor flow should be included in the tests. In this case, a full, cylindrical, can-type combustor including swirler, primary, secondary and dilution holes as well as the cooling holes are present in a Perspex flow visualisation combustor.

Experimental Setup

Test Rig

The gas turbine combustor test rig consists of a fan run by an 11 kW motor to supply the air for combustion. The fan is attached to a set of pipes, which house an orifice plate for flow rate measurement and allow the flow to develop, with the combustor liner placed at the end of the pipes at the outlet. The combustor then exhausts to atmosphere. Figure 1 shows a schematic diagram of the test rig.

The combustor liner is a generic can-type combustor which has a single swirler in the upstream dome end. The metal combustor used in the test rig for reacting tests is shown in Figure 2.

The transparent combustor shown in Figure 3 was manufactured such that the combustor liner inner diameters and holes were identical to the metal combustor. Due to the slightly thicker walls the outer diameter was not the same as the metal liner thus the annulus hydraulic diameter was matched. The transparent sections were manufactured from Perspex and the other plastic parts were manufactured from Ertacetal C.

The swirler is a 7 mm deep annular swirler with 10 flat vanes at 50° to the inlet plane. A detailed drawing of the swirler is shown in Figure 4. The primary, secondary and dilution zones have 6 x Φ9.5 mm, 8 x Φ5.0 mm and 10 x Φ11.8 mm holes respectively. Between the primary and secondary cylinders are 30 x Φ1.2 mm cooling holes and there are 50 x Φ1.2 mm cooling holes between the secondary and dilution cylinders. Figure 5 shows a detailed drawing of the Perspex combustor. The combustor liner fits inside a cylindrical casing with an inner diameter of 121.2 mm.

The experimental setup with the transparent combustor installed and the PIV equipment is shown in Figure 6.
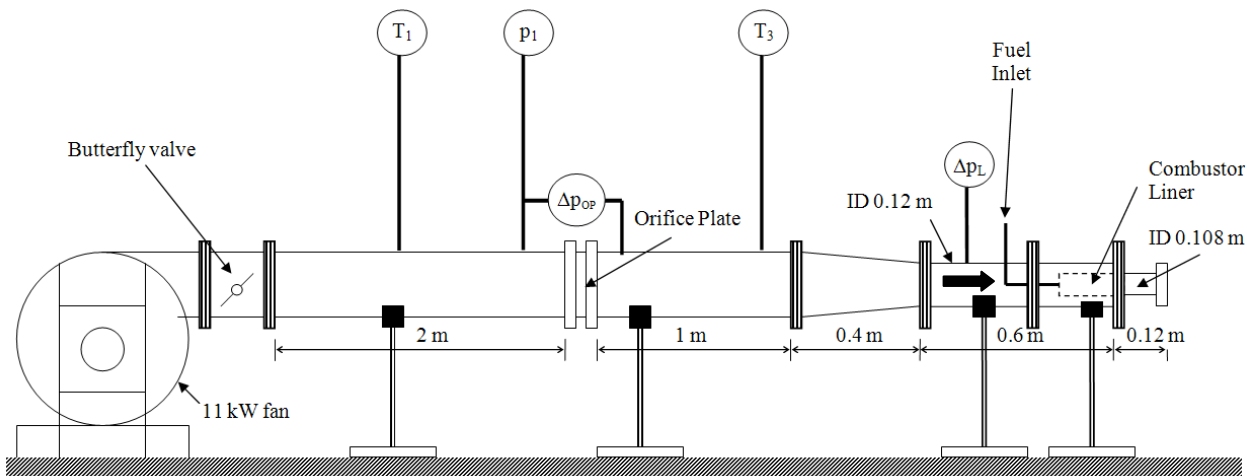

Figure 1: A schematic diagram of the test rig

Figure 2: The metal combustor liner

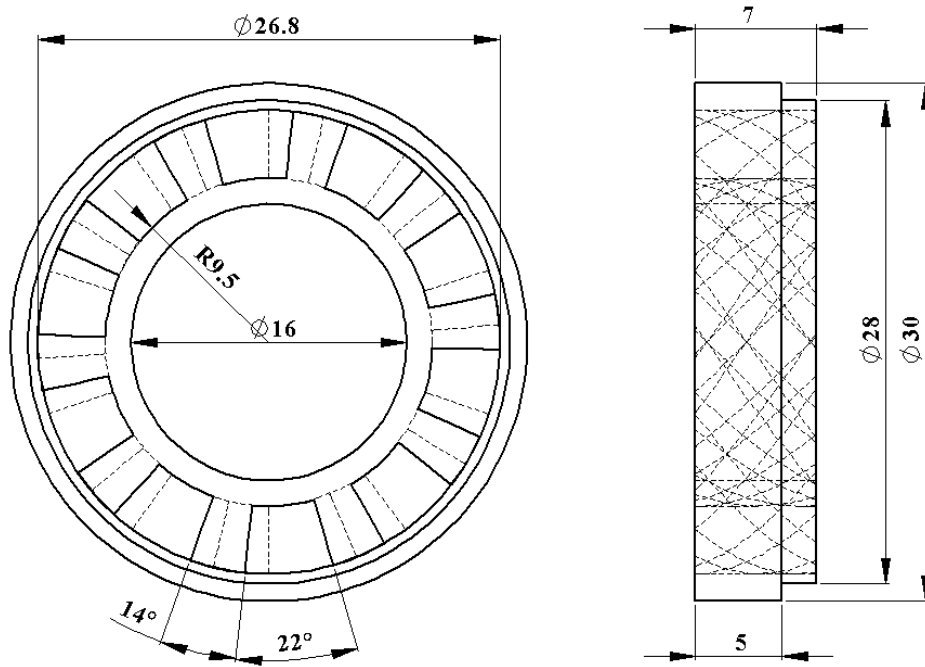**Figure 3: The transparent combustor parts - casing, liner and outlet pipe**

⌀26.8

7

R9.5

⌀16

⌀28 ⌀30

14° 22°

5

Figure 4: A detailed drawing of the swirler

230

174.1

124

104.5

79

60

19.2

6

1.6

5

5

⌀38

⌀30.4

4

4

⌀90.4
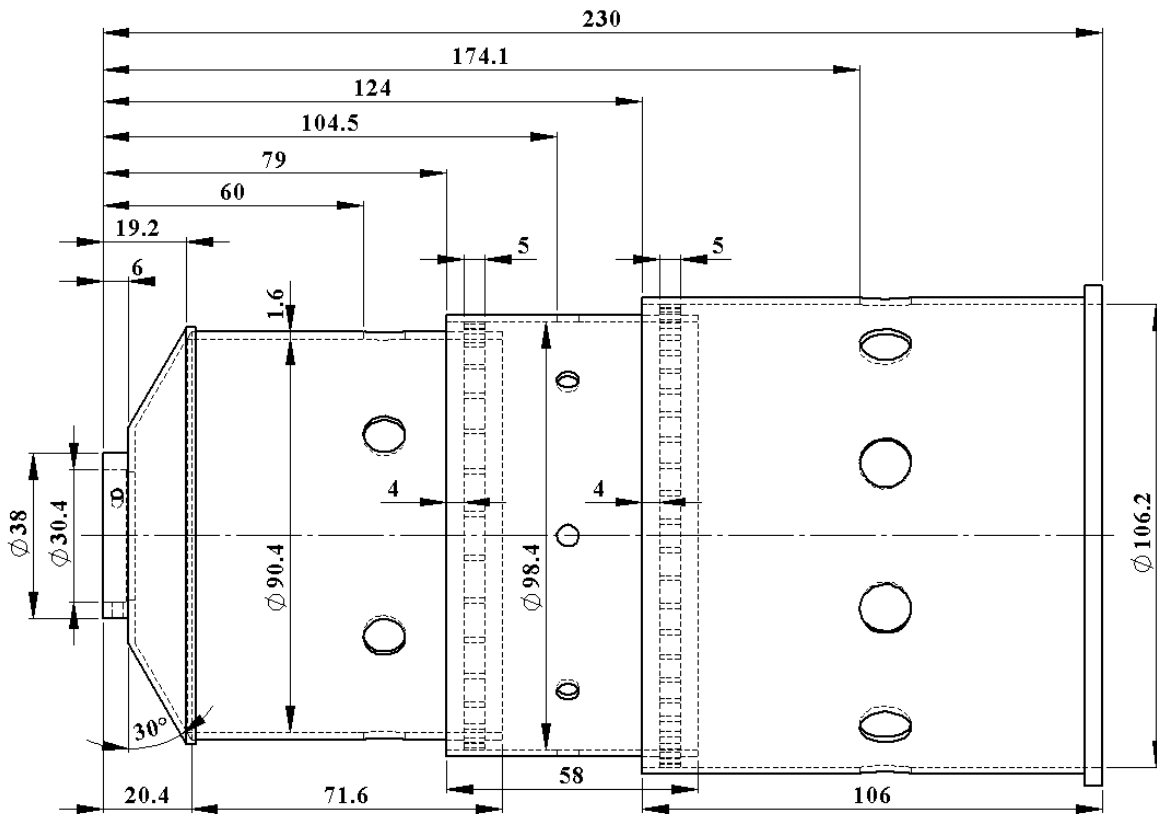
⌀98.4

⌀106.2

30°

20.4

71.6

58

106

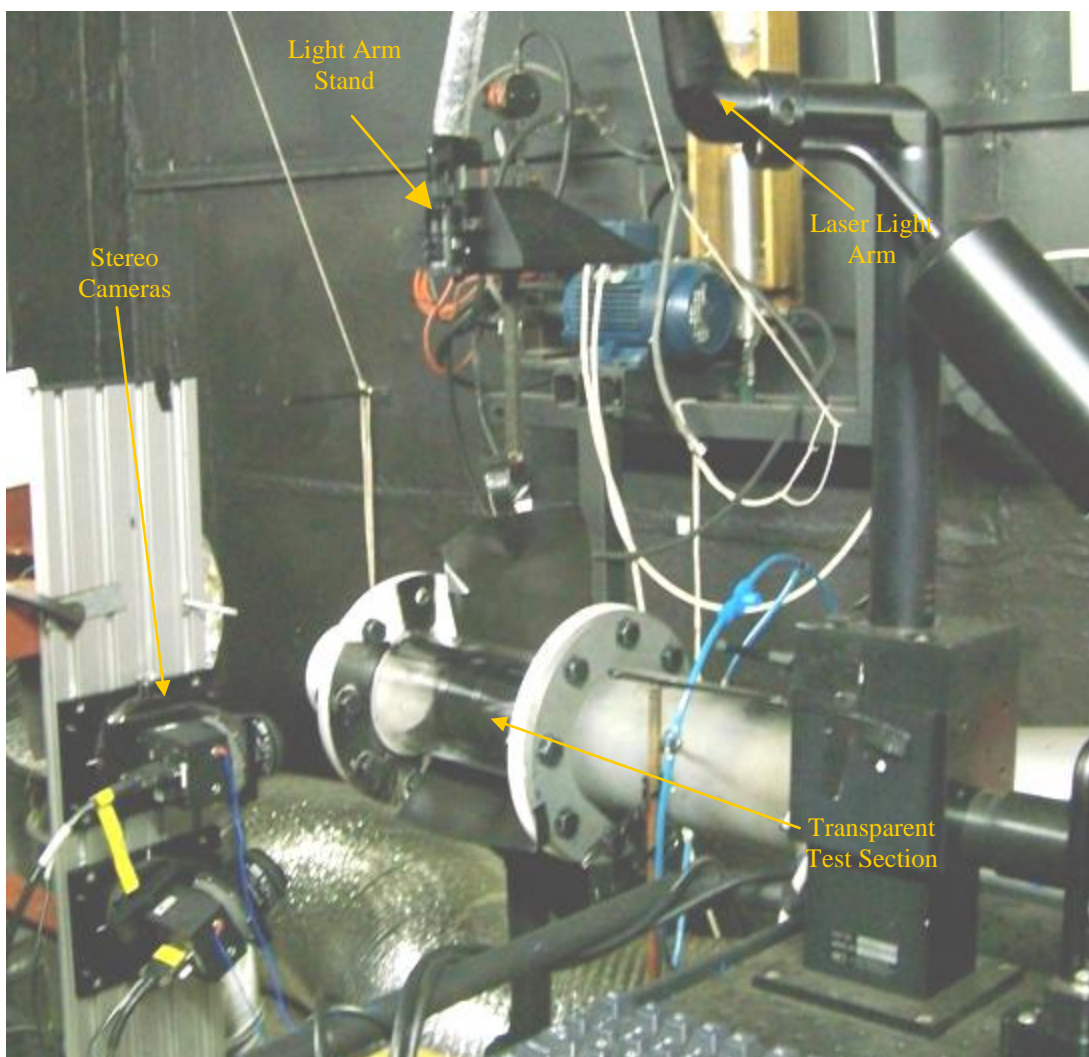**Figure 5: A detailed drawing of the Perspex combustor**

Figure 6: The transparent test section attached to the combustor test rig

Test Conditions

Each of the three zones of the combustor were tested separately with the laser sheet in line and in between the respective holes. Three-dimensional velocity vectors were obtained throughout the combustor. For each experiment the top camera was at 5° and the bottom camera at 20° to the normal of the laser sheet. The data presented here is for an air mass flow rate of 201.6 kg/h.

Instrumentation

A TSI stereoscopic PIV system was used for velocity field measurements. It has a dual laser head enabling a minimum of 1μs pulse separation time between laser flashes. The laser heads are Big Sky Laser CFR 200s attached to frequency doubling and alignment optics. These optics enable both laser heads to emit a beam through the same outlet and to convert the 1064 nm wavelength to a 532 nm wavelength. The laser beam is then passed into a laser arm which places the light in the required position. A -25 mm focal point cylindrical lens turns the beam into a sheet and a 500 mm focal point spherical lens focuses the sheet to give it a sheet thickness of approximately 1.5 mm in the test section. The laser sheet was aligned with the axial flow direction of the combustor liner.

The flow was seeded using smoke produced from burning oil. The cameras were required to be approximately 200 mm away from the combustor. This distance was chosen firstly to fill as much of the camera frame with the region of interest in the combustor as possible, and secondly because the smoke particles did not reflect light with enough intensity to place the cameras further away.

The two cameras used were Powerview 4M Plus greyscale CCD cameras each with a 2048 x 2048 pixel array. These cameras were then attached to a rail facing the test section with the Sheimflüg angle satisfied for PIV data collection. Both cameras were on the same side of the laser sheet with the top camera in back scatter and the bottom camera in forward scatter.

For each experiment 720 three-dimensional vector fields were averaged to get a steady state vector field. The TSI software Insight3G [7] was used to analyse the images captured and Tecplot [8] was used to average the data.

Uncertainty Analysis

Li and Gutmark [5] have stated that the uncertainty of PIV is greater than that of LDV which is taken as ±5% and thus was assumed to be of the order of ±5-10%.

In order to get an indication of the validity of the PIV data for this study, it was compared to a known technique of velocity measurement. A comparison of uniform flow coming out of the test rig without a liner was measured using a pitot tube and the PIV system. The velocity profile comparison is shown in Figure 7. The pitot tube velocity profile has error bands comprising of the instrument error of the pitot tube (±1.05%) and the uncertainty of the velocity due to the uncertainty involved with setting up a repeated air mass flow rate (±0.4%). The velocity profile at the same cross section obtained from an average of 735 PIV points per cell is plotted on the same graph. The scatter bands on the PIV profile show a 95% confidence interval for the PIV sample at each cell.
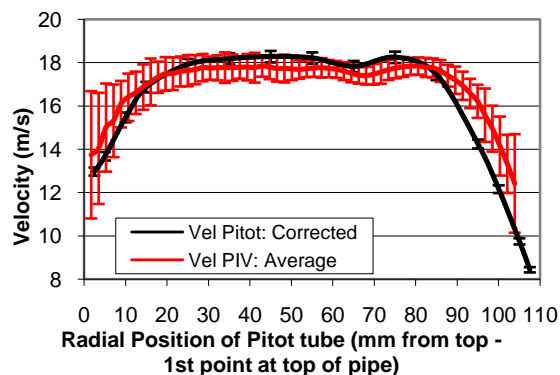

Figure 7: Comparison of the velocity profile at the outlet of the test rig

At the core of the flow the pitot tube and the PIV profile lie reasonably close with the pitot tube lying within the PIV scatter band which has an average of 3.2% in this region. Near the edge of the flow the PIV scatter bands increase in size because the flow on the edge of the jet is more unsteady than the core due to mixing with the ambient air. However, the profiles do follow a similar trend even at the edges of the flow.

Experimental Results

The velocity data was collected on a plane lying lengthwise along the central axis. This plane was chosen because it would encompass a large amount of information and it was one of the few orientations that would allow the cameras to be positioned such that large areas could be measured. The data on this plane is shown to be close to symmetrical throughout the length of the combustor.

In line with holes

The velocity magnitude contours and streamlines are shown in a normal view of the combustor liner in Figure 8a. This plane is aligned with the holes of all three zones. Figure 8b shows the three-dimensional velocity vector field on the same plane as Figure 8a and views from the upstream direction for each of the three zones.

In Figure 8a and 8b the primary zone return flow section can be seen at the core of the flow at (1). This region has flow velocities in the lower third of the velocity range. The jets are shown as yellow-green sectors on either side of the axial centerline (2). The primary zone jets penetrate to 100% of the radial distance into the flow. This is seen where the streamlines becoming asymptotic to the flow at the stagnation point. The symmetrical position of the swirling recirculation zone above and below the centerline in both figures is shown at (3). The returning flow zone shape can also be picked up here and it seems to be more rectangular rather than cone- or Y-shaped which are the more common shapes for a combustor recirculation zone [9].

Some of the more subtle features that can be observed in the vector field are: The bulk flow splitting off to enter the swirler at (4); The convergence of the bulk flow to enter the annulus around the combustor liner (5); The annulus flow curving into a primary zone hole to form a jet is also evident at (6); The flow in the annulus (7) and the remaining annulus flow converging into a smaller annulus around the next zone at (8).

At (3) in the upstream views in Figure 8b it is shown that the vectors are three-dimensional and that the fluid has a significant out-of-plane flow. This is expected due to the swirler. It can also be observed that for the half above the centerline, the vectors point to the left and to the right below the centerline. This shows that the flow is swirling. It also shows that the swirl velocity decreases as one moves away from the centre towards the liner wall. A summary of the primary zone features is listed in Figure 8a from (1) to (8).

1. Returning flow zone
2. Primary jets
3. Swirling recirculation flow
4. Bulk flow splitting into swirler
5. Bulk flow converging into annulus
6. Annulus flow entering holes into jets
7. Annulus flow
8. Annulus flow converging into a smaller annulus around secondary zone
9. Secondary jets
10. Forward flow region
11. Swirling flow
12. Annulus flow entering holes into jets
13. Annulus flow
14. Annulus flow converging into a smaller annulus around dilution zone
15. Returning flow zone
16. Recirculation zones
17. Dilution jets
18. Slight Swirling flow
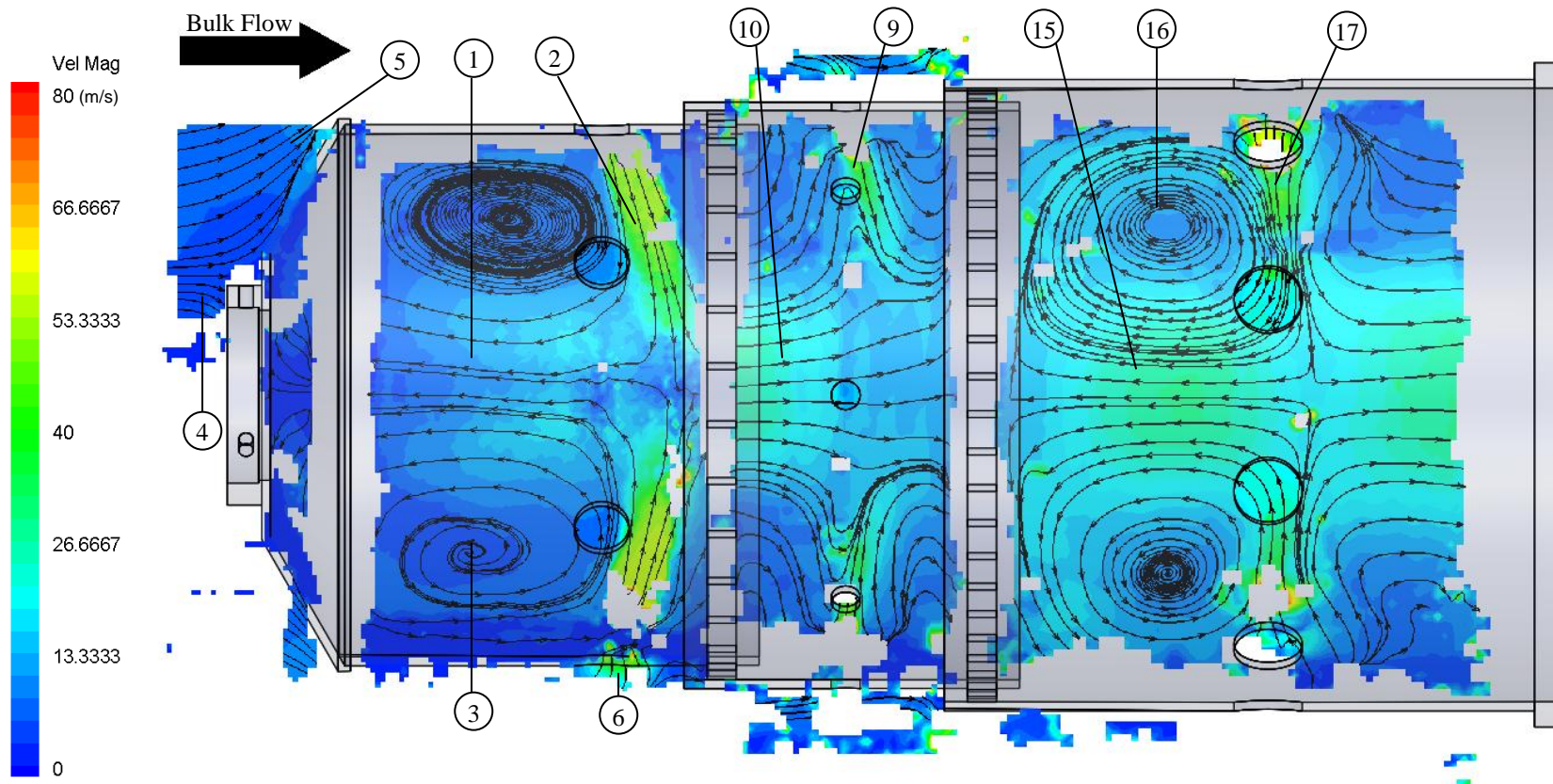
Figure 8a: A contour plot of velocity magnitude along with streamlines in line with the holes

Bulk Flow

⑦ ⑧ ⑬ ⑫ ⑭

⊗
Bulk Flow

③ ⑪ ⑱
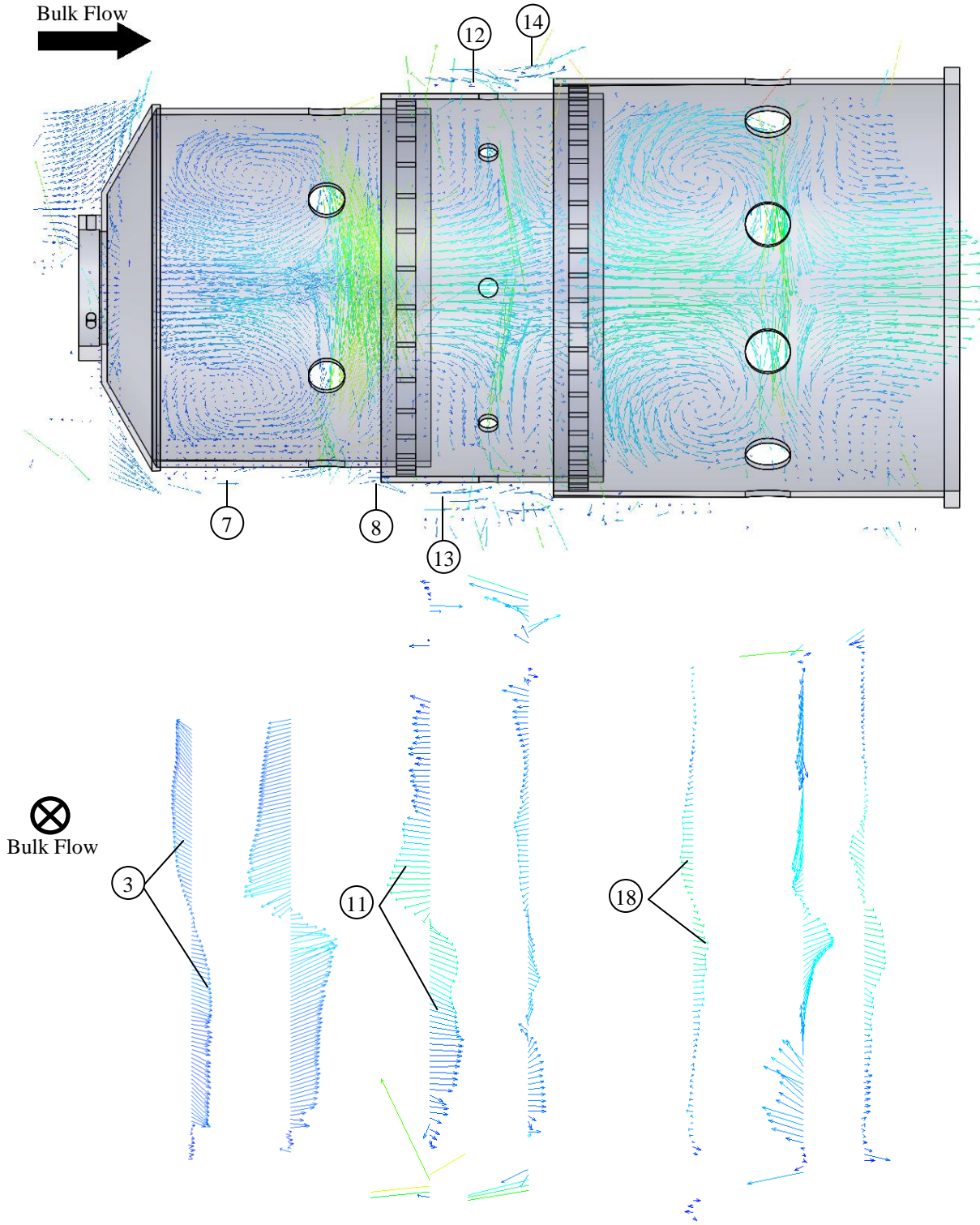
Key same as Figure 8a

Figure 8b: The velocity vector field in line with the holes viewed normal and from upstream for each zone

As with the primary zone, the secondary zone features are also listed in Figure 8a from (9) to (14). The secondary zone jets (9) only penetrate ±60% of the radial distance. This is expected due to the jets having a smaller portion (8.8%) of the total mass flow than the primary zone (22.5%) [10]. In the forward flow section, the outer part of the secondary zone flow diverges just before the jets, converges while passing the jets but then diverges again after the jets.

In the upstream view of the secondary zone the swirl (11) is shown to be less intense than in the primary zone. Similar features were observed in the annulus region as in the primary zone shown at (12), (13) and (14).

For the dilution zone results (16) shows that there is an unexpected recirculation zone with the centre flow in the reverse/return flow direction at (15). Furthermore, as with the primary zone jets, the dilution zone jets penetrate to 100% of the radial distance into the combustor (17). These jets receive the majority (50%) of the total mass flow but the hole set has a large number of large diameter holes so the velocity of the jet decreases at a faster rate than the primary jets [10].

Figure 8b shows that as the air progresses from the primary zone through the secondary zone and ending in the dilution zone, the swirling motion around the axis of the combustor becomes less intense and the axial and radial motion becomes dominant over the tangential flow. In the dilution zone there is only a slight swirl evident (18).

In between holes

In Figure 9a the planes are in between the holes of each of the respective zones. The primary zone plane is at 30° to the plane in line with the holes, the secondary zone is at 22.5° and the dilution zone is at 18°. All three planes are viewed normally. In this figure the velocity magnitude contours are shown with the streamlines superimposed.

Figure 9b shows the velocity vector field viewed from the side and the velocity vectors viewed from the upstream direction for each of the three zones.

In the primary zone, it is evident that the flow structure is very similar to the flow in line with the holes except that the jets are missing in this flow field. The features are pointed out at (19) to (24) in Figure 9a and Figure 9b.

The secondary zone flow in Figure 9a and 9b shows the central flow diverging outwards in the region where the jets were entering in the data set in line with the holes. Other than the lack of jets the flow field is again very similar to the flow with jets. Present in the secondary zone are the forward flow region (25) and swirling flow (26).

As in the previous two zones, in the dilution zone there are many of the same features in between the holes as in line with the holes and these are listed as (27) to (29). There is, however, a difference on the outer edges of the two recirculation zones in this section. The outer side of the recirculation zone leaves the vortex structure and flows along the wall to join the bulk flow of the combustor whereas in the plane inline with the holes the recirculating flow is blocked by the jets and remains in the vortex. This difference is shown in Figure 9a and 9b at (30).

Discussion

The results of the PIV experiment show a large amount of detail that enables the use of the data as an effective test case. The size and position of the recirculation regions can be used as an indicator for how well the turbulence model is performing in the simulation of both jets and swirling flow together. While the magnitude and shape of the tangential velocity profile is also a good tool to show how well the swirling flow was modelled. The recirculation region in the dilution zone, which is atypical, provides an additional test as to how well the CFD captures real flow features. The penetration depth of the jets is also a characteristic that should be well modelled using numerical techniques since the jet penetration can influence the rate of mixing in the combustor liner [11].

Summary

The three-dimensional velocity vector field was measured inside a transparent generic can-type gas turbine combustor using a stereoscopic PIV system. The data was captured on planes aligned with and in between the holes of each of the three sections of a can-type forward flow combustor.

The main flow features were captured such as the recirculation zones and jets. The more subtle features such as flow entering the swirler, entering holes from the annulus and converging into smaller annuli were also evident in some sections of the data.

An unexpected recirculation zone was observed in the dilution zone. The departure of the flow from the recirculation regions to join the bulk flow in the dilution zone was also shown.

This data can be used effectively as a test case for CFD due to the presence of all the flow features of the combustor.

Acknowledgements

19. Returning flow zone
20. Swirling recirculation flow
21. Bulk flow splitting into swirler
22. Bulk flow converging into annulus
23. Annulus flow
24. Annulus flow converging into a smaller annulus around secondary zone

25. Forward flow region
26. Swirling flow

27. Returning flow zone
28. Recirculation zones
29. Slight swirling flow
30. Flow leaving the recirculation zone
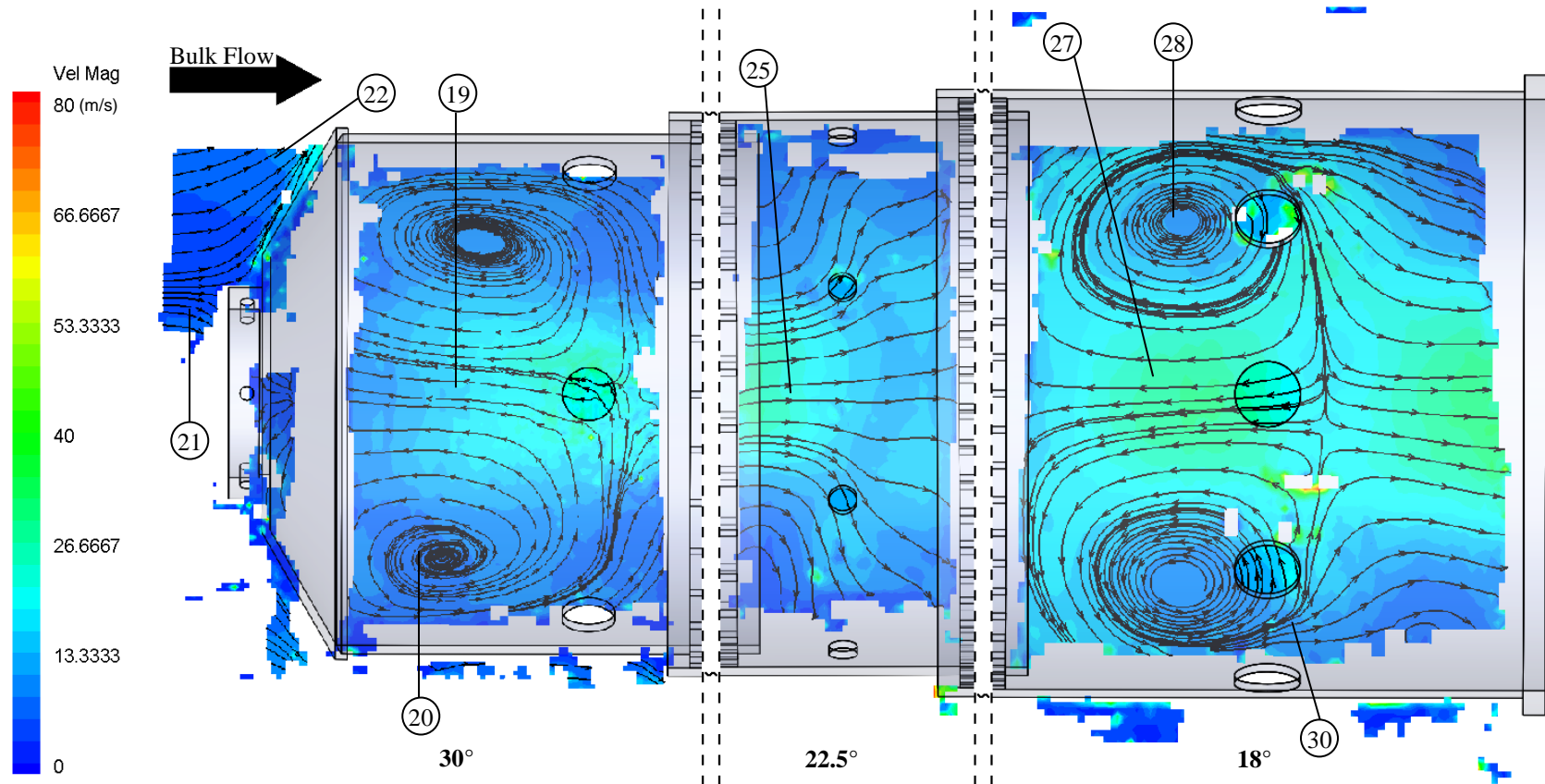
Figure 9a: A contour plot of velocity magnitude along with streamlines in between the holes

Bulk Flow

30° ㉓ ㉔   **22.5°**   **18°** ㉚

Bulk Flow

㉑   ㉖   ㉙
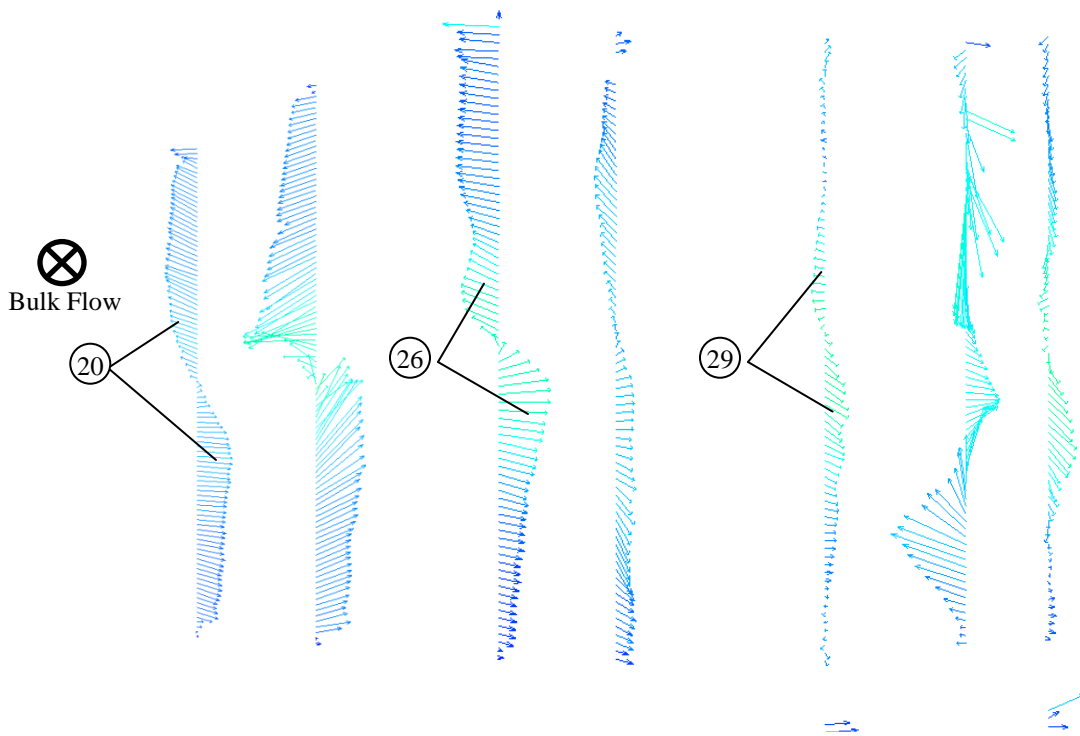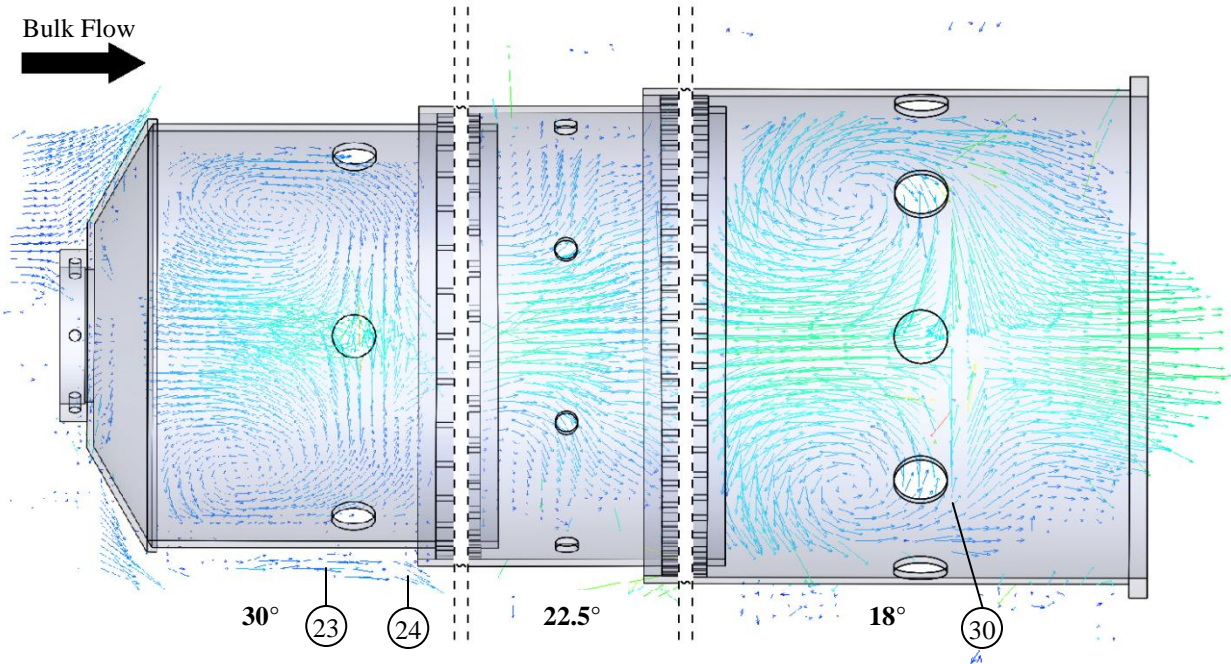
Key same as Figure 9a

Figure 9b: The velocity vector field in between the holes viewed normal and from upstream for each zone

References

[1] Vakil, SS., Thole, KA., 'Flow and Thermal Field Measurements in a Combustor Simulator Relevant to a Gas Turbine Aeroengine', *Journal of Engineering for Gas Turbines and Power*, Vol. 127, pp 257-267, April 2005

[2] Archer, S., Gupta, AK., 'Confinement Effects on Flow and Combustion under Fuel Lean Conditions', *Proceedings of IMECE04 2004 ASME International Mechanical Engineering Congress and Exposition,* Anaheim, California, USA, IMECE2004-60930, November 2004

[3] Mandai, S., Nishida, H. 'Application of Turbulent Reacting Flow Analysis for Gas Turbine Combustor Development', *JSME International Journal*, Series B, Vol. 47, No. 1, 2004

[4] Janus, B., Dreizler, A., Janicka, J., 'Flow Field and Structure of Swirl Stabilized Non-Premixed Natural Gas Flames at Elevated Pressure', *Proceedings of ASME Turbo Expo 2004 Power for Land, Sea, and Air*, Vienna, Austria, GT2004-53340, June 2004

[5] Li, G., Gutmark, EJ., 'Boundary Condition Effects on Nonreacting and Reacting Flows in a Multiswirl Combustor', *AIAA Journal*, Vol. 44, No. 3, pp 444 – 456, March 2006

[6] Carl, M., Behrendt, T., Fleing, C., Frodermann, M., Heinze, J., Hassa, C., Meier, U., Wolff-Gassmann, D., Hohmann, S., Zarzalis, N., 'Experimenal and Numerical Investigation of a Planar Combustor Sector at Realistic Operating Conditions', *Journal of Engineering for Gas Turbine and Power*, Vol. 123, pp 810-816, October 2001

[7] TSI Incorporated, 'INSIGHT 3G™ Data Acquisition, Analysis, and Display Software User's Guide', P/N 1980511, Revision C, United States of America, September 2005

[8] Tecplot Incorporated, Tecplot v 10.0-6-012, United States of America, 1988

[9] Li, G., Gutmark, EJ., 'Geometry Effects on the Flow Field and the Spectral Characteristics of a Triple Annular Swirler', *Proceedings of ASME Turbo Expo 2003 Power for Land, Sea and Air,* Atlanta, Georgia, USA, GT2003-38799, June 2003

[10] Meyers, B C., 'The Design, Manufacture and Testing of the Dilution Zone of a Gas Turbine Combustor', *Final Year Project Report at Department of Mechanical and Aeronautical Engineering, University of Pretori,* South Africa, 2003

[11] Lefebvre, A H., 'Gas Turbine Combustion', *Hemisphere Publishing Corporation,* 1983. ISBN 0-89116-896-6